

See discussions, stats, and author profiles for this publication at: <https://www.researchgate.net/publication/263938749>

Self-Assembly in Poly(dimethylsiloxane)-Poly(ethylene oxide) Block Copolymer Template Directed Synthesis of Linde Type A Zeolite

ARTICLE in LANGMUIR · MAY 2013

Impact Factor: 4.46 · DOI: 10.1021/la400951s

CITATIONS

5

READS

42

6 AUTHORS, INCLUDING:



Pietro Calandra

Italian National Research Council

52 PUBLICATIONS 646 CITATIONS

[SEE PROFILE](#)



Mikhail Alekseyevich Kiselev

Joint Institute for Nuclear Research

63 PUBLICATIONS 1,212 CITATIONS

[SEE PROFILE](#)



Heinz Amenitsch

Graz University of Technology

375 PUBLICATIONS 8,375 CITATIONS

[SEE PROFILE](#)



Domenico Lombardo

Italian National Research Council

47 PUBLICATIONS 594 CITATIONS

[SEE PROFILE](#)

Self-Assembly in Poly(dimethylsiloxane)-Poly(ethylene oxide) Block Copolymer Template Directed Synthesis of Linde Type A Zeolite

Lucio Bonaccorsi,[†] Pietro Calandra,[‡] Mikhail A. Kiselev,[§] Heinz Amenitsch,^{||} Edoardo Proverbio,[†] and Domenico Lombardo*,[‡]

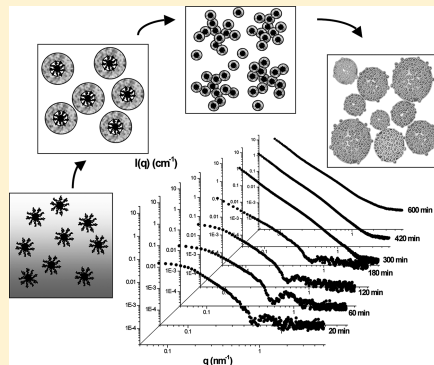
[†]Dipartimento di Chimica Industriale e Ingegneria dei Materiali, Università di Messina, Salita Sperone 31, I-98166 Sant'Agata (Messina), Italy

[‡]Istituto per i Processi Chimico Fisici (IPCF) (Sezione di Messina), Consiglio Nazionale delle Ricerche (CNR), Viale F. Stagno D'Alcontres 37, I-98158 Messina, Italy

[§]Frank Laboratory of Neutron Physics, Joint Institute for Nuclear Research, Dubna, Moscow Region, Russia

^{||}Institute of Biophysics and Nanosystems Research, Austrian Academy of Sciences, Schmiedlstrasse 6, 8042 Graz, Austria

ABSTRACT: We describe the hydrothermal synthesis of zeolite Linde type A (LTA) submicrometer particles using a water-soluble amphiphilic block copolymer of poly(dimethylsiloxane)-*b*-poly(ethylene oxide) as a template. The formation and growth of the intermediate aggregates in the presence of the diblock copolymer have been monitored by small-angle X-ray scattering (SAXS) above the critical micellar concentration at a constant temperature of 45 °C. The early stage of the growth process was characterized by the incorporation of the zeolite LTA components into the surface of the block copolymer micellar aggregates with the formation of primary units of 4.8 nm with a core–shell morphology. During this period, restricted to an initial time of 1–3 h, the core–shell structure of the particles does not show significant changes, while a subsequent aggregation process among these primary units takes place. A shape transition of the SAXS profile at the late stage of the synthesis has been connected with an aggregation process among primary units that leads to the formation of large clusters with fractal characteristics. The formation of large supramolecular assemblies was finally verified by scanning electron microscopy, which evidenced the presence of submicrometer aggregates with size ranging between 100 and 300 nm, while X-ray diffraction confirmed the presence of crystalline zeolite LTA. The main finding of our results gives novel insight into the mechanism of formation of organic–inorganic mesoporous materials based on the use of a soft interacting nanotemplate as well as stimulates the investigation of alternative protocols for the synthesis of novel hybrid materials with new characteristics and properties.



1. INTRODUCTION

The construction of supramolecular organic–inorganic nanostructures based on porous materials has been drawing increasing attention for its ease of use and high efficiency to create mesoporosity.^{1–4} The goal of the different strategies is to achieve a synergy between the properties originating from the porous inorganic substrate and the properties of the involved organic components. Particularly stimulating is the study of alternative protocols for the assembly mechanism of such materials in which a macromolecular template drives the formation of nanostructures with peculiar final properties. In the form of a molecular, colloidal, or polymeric precursor, the template furnished the conditions for a favorable adaptability to the involved self-assembly process. In this respect the use of block copolymer self-assembly has been demonstrated to be one of the promising bottom-up methods for the design and construction of hybrid inorganic–organic functional nanomaterials.^{5–8} In these systems, in fact, the thermodynamic incompatibility between the different blocks causes a microphase separation that gives rise to a spatial organization of morphologies starting from the nano-

meter scale. By modifying the system volume fraction and solution conditions, novel structural transitions can be induced as demonstrated by different studies.^{9–13} In this respect the combination of supramolecular interactions^{14–17} and the ability to control both the length scale and the structural morphologies makes block copolymers particularly attractive templates in the synthesis of nanoporous materials with new characteristics and properties.^{18–22}

Herein, we describe the formation of submicrometer particles of zeolite Linde type A (LTA) grown on a poly(dimethylsiloxane)-*b*-poly(ethylene oxide) (PDMS-*b*-PEO) diblock copolymer used as a templating agent. Owing to their size selectivity properties, LTA zeolites are used in many applications such as solid acid catalysts, household products, agriculture, and water treatment.²³ They are obtained by means of a gelling process during a hydrothermal synthesis, where aluminosilicate

Received: March 13, 2013

Revised: May 2, 2013

Published: May 7, 2013

components are heated to the crystallization of the zeolite.²⁴ The use of block copolymers as template agents allows the choice of the size and composition of the core substrate as well as modulation of the main feature of the soft interaction at the boundary between organic and inorganic domains. More specifically, the choice of the PDMS-*b*-PEO block copolymer template relies on the formation of micellar aggregates characterized of highly ramified PEO chains, which are responsible for the formation of a network of water molecules all around the macromolecular template.²⁵ In this sense the water coordination around the precursor aggregates may promote a condensed growth of the zeolitic phase onto the copolymer substrate. Moreover, the long PEO chains ensure an enhanced stability of the micellar aggregates generated at concentrations higher than the critical micellar concentration (cmc).

2. EXPERIMENTAL SECTION

2.1. Materials. The zeolite synthesis mixtures, prepared according to the standard procedure,^{23,24} had the following molar ratio: 2.0NaO₂:1Al₂O₃:1.9SiO₂:65H₂O. The PDMS-*b*-PEO diblock copolymer of molecular weight $M_w = 5000$ was composed of 82 wt % PEO (obtained from SP2 Polymer Canada and further purified). The polydispersity index after purification was $M_w/M_n = 1.15$ (where M_w is the weight-average molecular weight and M_n is the number-average molecular weight of the copolymer). The PEO-*b*-PDMS block copolymers were dispersed in deionized water, while the obtained solutions were filtered with Teflon filters (the pore diameter D was 0.02 μm). The solutions were also checked by dynamic light scattering prior to small-angle X-ray scattering (SAXS) measurements to remove the possible presence of aggregates in the system. All zeolite LTA reactants were preliminarily mixed and diluted in water (dilution factor 1:20, w/w) and then added with an equal weight of a water solution of PEO-*b*-PDMS at concentration $c = 0.04 \text{ g/cm}^3$. In a clear solution no gel formation is visible to the naked eye due to the high reactant dilution, so the usual formation of polycrystalline aggregates observed in zeolite grown from a dense gel is largely slowed. Hydrothermal synthesis of zeolite LTA in the presence of the PEO-*b*-PDMS block copolymers has been performed at a constant $T = 45^\circ\text{C}$.

2.1. Methods. **2.2.1. Small-Angle X-ray Scattering.** The small-angle X-ray scattering experiments during the zeolite growth process were performed at $T = 45^\circ\text{C}$ on the 5.2L beamline at the Elettra Synchrotron Light Laboratory, Trieste, Italy.^{26,27} The energy and wavelength of the incident X-ray beam were 8 keV and 1.54 \AA , respectively. The beam size was 2 mm \times 0.8 mm, while the SAXS intensity was measured on a 2D charge-coupled device (CCD) detector (Photonic Science, Oxford, U.K.). The range of SAXS scattering vector covered was $0.07 \text{ nm}^{-1} < q < 5 \text{ nm}^{-1}$. The scattering data were normalized with respect to transmission and were corrected by the empty cell and solvent contributions.

2.2.2. Light Scattering. For the determination of the cmc, we used a Malvern light scattering apparatus with a duplicate Nd:yttrium-aluminum-garnet laser (with a vacuum wavelength $\lambda_0 = 532 \text{ nm}$) at a power of 200 mW. Measurements have been performed at a constant $T = 45^\circ\text{C}$. The upper cloud consolute point (UCCP) of the block copolymer varies in the range of 58–65 $^\circ\text{C}$ for concentration values between 0.01 and 0.3 g/cm^3 . The refractive index increment $dn/dc = 0.13 \text{ cm}^3/\text{g}$ has been measured using a homemade differential refractometer below the UCCP in the temperature range of $15 < T < 45^\circ\text{C}$, and it does not depend on the temperature.

2.2.3. Scanning Electron Microscopy. Electron microscopy was performed using a scanning electron microscope (JEOL 5600LV) operating at 10 kV in low-vacuum conditions. The microscope was equipped with a backscattered electron detector and an energy-dispersive spectroscopy (EDS) electronic microprobe (SEMQuant, Oxford, U.K.). Samples of the reactant solution were left drying overnight at room temperature and then gathered on specimen stubs and submitted to the analysis.

3. RESULTS AND DISCUSSION

The first investigation in the present work involves the determination of the cmc value for the water solution of the PDMS-PEO copolymer at $T = 45^\circ\text{C}$. This determination implies the measurement of the absolute excess scattered intensity R as a function of the exchanged wave vector $q = (4\pi n/\lambda_0) \sin(\theta/2)$ and the optical constant $K = (4\pi n^2/\lambda_0 N_A)(dn/dc)^2$:

$$R(q) = KM_w cP(q) S(q) \quad (1)$$

where $P(q)$ and $S(q)$ are the normalized form factor and the structure factor, respectively, M_w is the molecular weight, c is the mass concentration, θ is the scattering angle, n is the refractive index of the solution, λ_0 is the wavelength of light in a vacuum, dn/dc is the refractive index increment with concentration, and the N_A is the Avogadro number. Measuring the absolute intensity Kc/R^{90° at scattering angle $\theta = 90^\circ$ as a function of concentration, a minimum has been detected at the critical micelle concentration $c_{\text{cmc}} = 0.007 \text{ g/cm}^3$, thus indicating that a micellization process takes place (Figure 1).

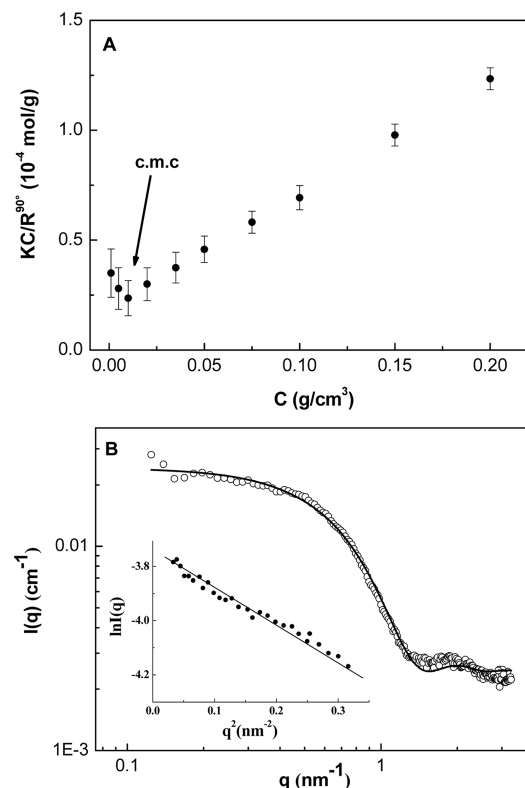


Figure 1. Normalized inverse excess scattered intensity at 90° as a function of concentration at $T = 45^\circ\text{C}$. The arrow indicates the value of the cmc, above which micelles are present in the system (A). SAXS form factor analysis at $T = 45^\circ\text{C}$ for the PDMS-PEO block copolymer in water solution at $c = 0.04 \text{ g/cm}^3$ (B). In the inset the corresponding Guinier analysis for the form factor is presented.

To obtain preliminary structural information on the employed template at $T = 45^\circ\text{C}$, an SAXS experiment has been carried out in a water solution of PEO-*b*-PDMS at $c = 0.04 \text{ g/cm}^3$. Assuming the absence of interparticle interaction (i.e., $S(q) = 1$), the SAXS intensity $I(q)$ can furnish direct information on morphological features of the block copolymer micellar aggregates. The fit of SAXS data with the form factor of a sphere of radius R [$I(q) =$

$I(0)[3J_1(qR)/(qR)]^2$ (where $J_1(x) = [\sin(x) - x \cos(x)]/x^2$ is the first-order spherical Bessel function)²⁹] has furnished a value of the PEO-*b*-PDMS micellar radius R of 2.87 nm (Figure 1B). The micelle radius of gyration $R_g = 1.93$ nm has also been obtained from the slope of $\ln I(q)$ vs q^2 (inset of Figure 1B) in the so-called Guinier region (i.e., for $qR_g < 1$), where the particle form factor can be expressed as $I(q) = I(0) \exp(-q^2 R_g^2/3)$.²⁹ The deviation between R and R_g can be attributed to the highly ramified conformation of copolymer micelles. Useful information about the micellar aggregation number can be obtained from the laser light scattered intensity at scattering angle $\theta = 90^\circ$ through the virial expansion²⁸

$$\frac{K(c - c_{cmc})}{R^{90^\circ} - R_{cmc}^{90^\circ}} = \frac{1}{M_w} [1 + 2A_2 M_w (c - c_{cmc})] \quad (2)$$

where R^{90° is the absolute excess scattered intensity at scattering angle $\theta = 90^\circ$ and A_2 is the static virial coefficient. In Figure 2 the

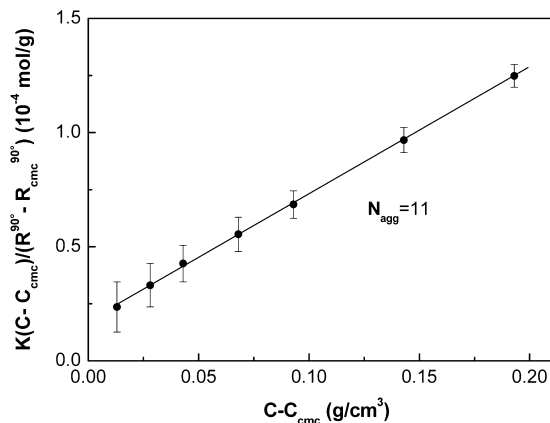


Figure 2. Normalized inverse absolute intensity of micelles as a function of copolymer concentration at $T = 45$ °C. In the figure the mean aggregation number N_{agg} of the micelles is reported.

Debye plot is reported as a function of the PDMS–PEO block copolymer concentration. From a linear fit a micelle molecular weight $M_w = 55\,000$ is obtained, which corresponds to a mean micelle aggregation number $N_{\text{agg}} = 11$. The aggregation number is very small in comparison with most results reported in the literature on block copolymers, and it can be explained as a direct consequence of the relatively long PEO chain. The hydrophilic part of the copolymer chain, in fact, constitutes more than 80% of its total mass; the geometrical packing, therefore, requires a low aggregation number to screen the hydrophobic PDMS segments from the contact of water.

To investigate the self-assembly process during LTA particle formation in the presence of PEO-*b*-PDMS block copolymer, SAXS experiments have been performed at a constant $T = 45$ °C as a function of time after the mixing of the main reactants (Figure 3). A progressive increase in the SAXS scattering intensity in the small q range, as a function of the elapsed time, can be traced back to the growth process during zeolite formation. More specifically, during the early stage of the synthesis, while a Guinier type behavior is present in the low scattering wavevector range (i.e., for $q < 0.2$ nm⁻¹), the presence of pronounced oscillations in the high q range (i.e., for $q > 0.3$ nm⁻¹) can be connected to an internal interference caused by intraparticle contrast effects. Assuming the formation of aggregates composed of a block copolymer core and the growing zeolite in a surrounding shell, the corresponding form factor can thus be described by a core–shell model expressed as a function of the core and shell radii, R_1 and R_2 , respectively, and core and shell scattering-length densities, ρ_c and ρ_s . The scattering-length density (SLD) is expressed as $\rho = \sum_i b_i/V$, where V is the volume of the core or shell region while b_i is the scattering length of the corresponding component atoms. The corresponding form factor $P(q)$ (spherical core–shell model) can be expressed as²⁹

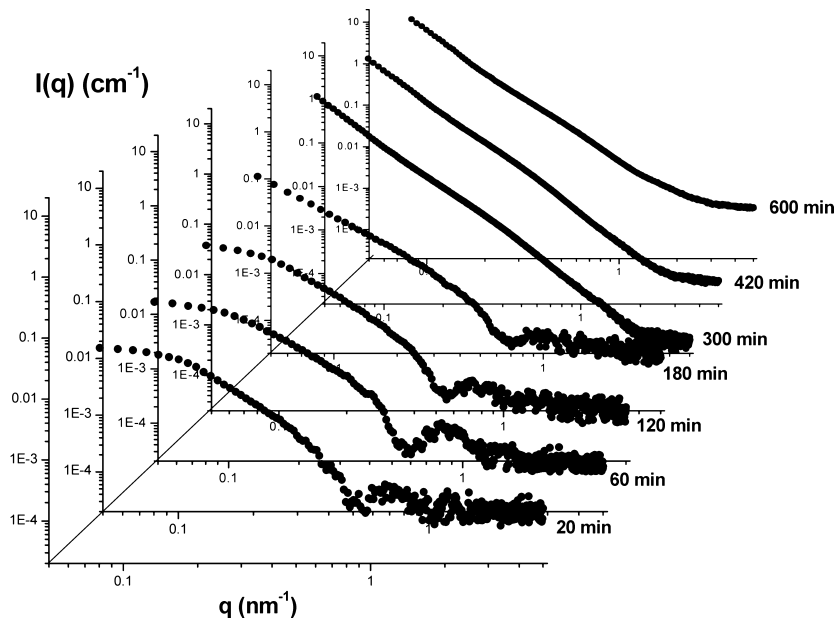


Figure 3. Evolution of the SAXS intensity profile of the PDMS–PEO block copolymer (at a water concentration $c = 0.04$ g/cm³) in the presence of the mother liquor for the LTA zeolite synthesis. SAXS profiles at different elapsed times after mixing (from 20 to 900 min) have been recorded at a synthesis temperature $T = 45$ °C.

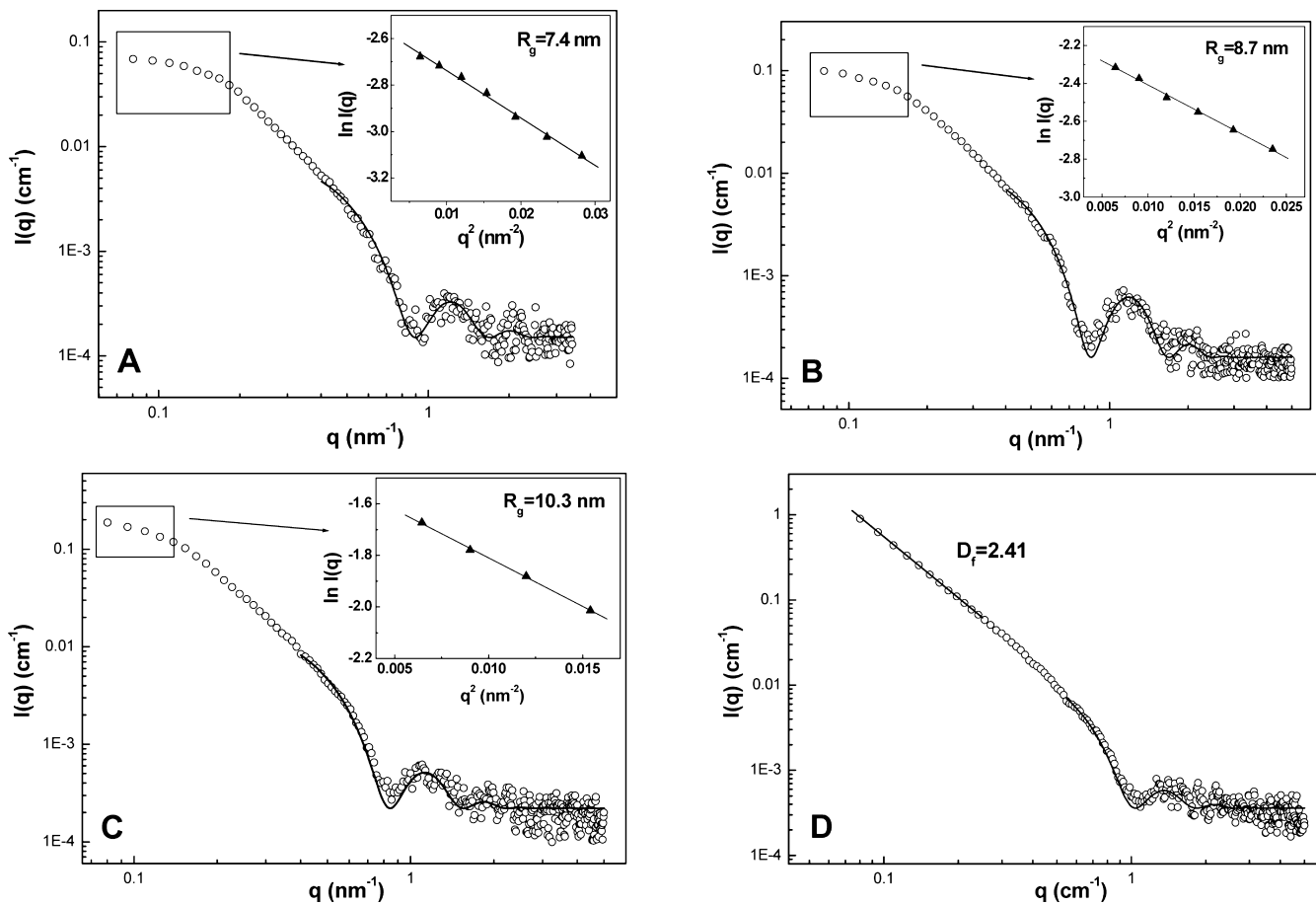


Figure 4. SAXS data analysis during the early stage of the LTA zeolite synthesis. While a Guinier-type analysis is performed for scattering wavevector $q < 0.15$ nm $^{-1}$ (see the insets in (A)–(C)), a core–shell approach is adopted for $q > 0.3$ nm $^{-1}$. (D) Linear behavior in the low q region of the log–log plot of the SAXS intensity is connected with a fractal characteristic of the particles.

$$P(q)(\Delta\rho)^2 = \left[\frac{4\pi}{3} R_1^3 (\rho_c - \rho_s) \frac{3J_1(qR_1)}{qR_1} + \frac{4\pi}{3} R_2^3 (\rho_s - \rho_0) \frac{3J_1(qR_2)}{qR_2} \right]^2 \quad (3)$$

where $J_1(x) = [\sin(x) - x \cos(x)]/x^2$ is the first-order spherical Bessel function. The a priori determination of SLD is complicated by the presence of complex chemical heterogeneity and density variation within a concentrated medium of sols, together with a complex hydration process involved in both regions that produces the shift of the corresponding effective SLD toward that of the solution medium. A linear behavior in the low q region of the log–log plot of the SAXS intensity at an elapsed time $t = 120$ min is detected (Figure 4D). This circumstance is connected with a fractal characteristic of the generated aggregates, while from the slope a fractal dimension $D_f = 2.41$ is obtained. The summary of the results obtained by the SAXS fitting procedure, reported in Figure 5, indicates average values for the core radius $R_1 = 2.61$ nm and shell radius $R_2 = 4.83$ nm, both remaining nearly constant during the LTA synthesis. On the contrary, an increase in the gyration radius R_g is detected, which passes from $R_g = 7.4$ nm (at $t = 20$ min) to $R_g = 8.7$ nm (at $t = 60$ min) up to $R_g = 10.3$ nm (at $t = 120$ min). The obtained SAXS results allow a hypothesis to be made about the formation mechanism of the zeolite LTA in the presence of the PDMS-*b*-PEO diblock copolymer micellar aggregates. The early stage of

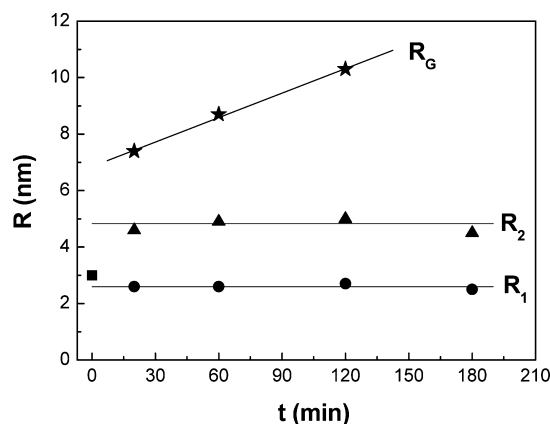


Figure 5. Evolution of the average core radius R_1 , shell radius R_2 , and gyration radius R_g as a function of the elapsed time during the early stage of the LTA synthesis in the presence of PEO-*b*-PDMS copolymer. Lines are guides for the eyes, while uncertainties are of the same order as the symbol sizes in the graph.

the growth process is characterized by the incorporation of the zeolite aluminosilicate components into the surface of the nanotemplate with the formation of primary units with a core–shell morphology. This growth process is restricted to an initial time between 1 and 3 h during which the core–shell structure does not show significant changes (R_1 and R_2 nearly constant), while a contemporaneous aggregation process among primary units

can be correlated with the detected increase in R_g as a function of the elapsed time during hydrothermal synthesis. The shape transition of the SAXS curve in the low q region occurring for the elapsed time of 180 min (see Figure 4D) can be connected with the formation of fractal aggregates between primary units. More specifically, the slope α of $\log I(q)$ vs $\log q$ identifies a linear region which is typical of the presence of extended fractal aggregates, with a fractal dimension given by $D_f = \alpha = 2.41$, which is near the value of $D_f = 2.53$ corresponding to the fractal dimension obtained during the diffusion-limited aggregation (DLA) regime,³⁰ where diffusing particles irreversibly adhere to form clusters with a branched structure. The fractal dimension of a particle, in fact, can be determined by analyzing the power-law regime of the scattered intensity $I(q) \approx q^{-\alpha}$, where the exponent α is related to the fractal dimension D of the scattering structures.³⁰ For a mass fractal in a three-dimensional space $\alpha_m = D_m$ and $1 < \alpha < 3$, whereas for surface fractals $\alpha = 6 - D_s$. For a smooth interface with nonfractal structures the well-known Porod's law $I(q) \propto q^{-4}$ (i.e., $D_s = 2$) holds.

Concerning the late stage of the synthesis, the slope of $\log I(q)$ vs $\log q$ identifies three linear regions of SAXS curves (Figure 6).

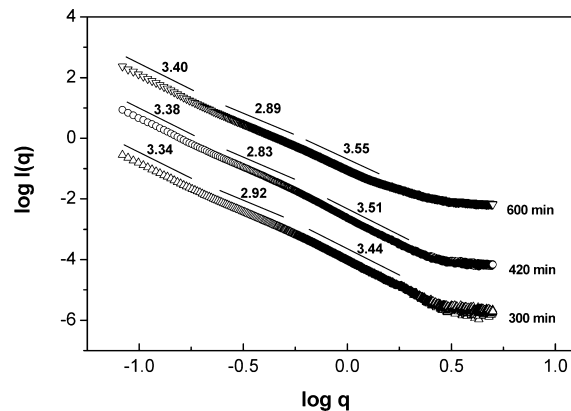


Figure 6. log–log plot of the SAXS intensity profile during the late stages of LTA zeolite synthesis for the system containing PDMS–PEO block copolymer at a water concentration $c = 0.04 \text{ g/cm}^3$. The curves have been vertically shifted for a better inspection.

Those regions correspond respectively to a mass fractal in the intermediate region of the scattering wavevector, $0.20 < q < 0.65 \text{ nm}^{-1}$, with an average slope $\alpha = 2.88$ (corresponding to a mass fractal dimension $D_m = 2.88$) and a surface fractal at the two extremes of the wavevector q ranges with average slopes $\alpha_1 = 3.37$ (low q region) and $\alpha_2 = 3.50$ (high q region), corresponding to surface fractal dimensions $D_{s1} = 2.63$ and $D_{s2} = 2.50$, respectively. These results furnish a first indication of the presence of different boundaries separating the fractal nature of the aggregates generated in different stages of the synthesis. The scaling range of the mass fractal aggregates (within which SAXS spectra exhibit a straight line) is limited from above by the size of the basic building units $d_u = 2R_2$ (in our case $R_2 = 4.83 \text{ nm}$ is the average shell radius) detected during the early stage of the synthesis process. This allows a cutoff value of $q_{m2} = 2\pi/d_u = 0.65 \text{ nm}^{-1}$ to be addressed, which corresponds to the upper q limit in the linear region of the SAXS curves (Figure 6). On the other hand, the lower value of $q_{m1} = 2\pi/d_{agg}$ delimiting from above the range of the linear behavior in the low q region, is influenced by the presence of large aggregates. In the case of systems containing particles of different sizes, generated as in our case by a self-assembly process among primary units, the SAXS analysis is

complicated by the fact that the head portion of the curves for the scattering of small particles falls within the scattering region of large particles.

The formation of large supramolecular assemblies at the late stage of the synthesis process was finally confirmed by scanning electron microscopy (SEM) experiments, as shown in Figure 7.

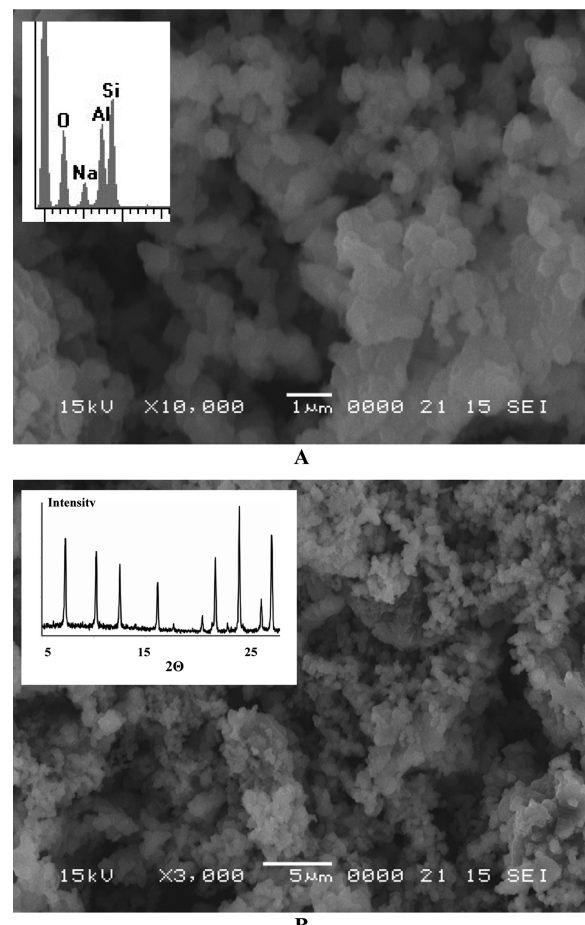


Figure 7. Scanning electron microscopy image of the aggregates generated during hydrothermal treatment at $T = 45^\circ\text{C}$ of LTA zeolite synthesis in the presence of the PDMS–PEO block copolymer system. The backscattered SEM image of the system confirmed condensation of the aluminosilicate components on the aggregate surfaces as proved by EDX microprobe analysis (inset of (A)). The analysis of the position of the X-ray diffraction peaks indicates the presence of the zeolite LTA (inset of (B)).

The figure shows the presence of large polydisperse spherical aggregates with sizes in the range of $100 < d_{agg} < 300 \text{ nm}$. The backscattered SEM image of the system confirmed a condensation of the aluminosilicate components on the aggregate surfaces as proved by the energy-dispersive X-ray (EDX) microprobe analysis (inset of Figure 7A). To confirm the nature of the condensate phase, the synthesis solution was left reacting at room temperature for 8 days and then was dried at 45°C for 24 h. The solid was collected and dried again at 80°C for 12 h and checked by powder X-ray diffraction (XRD). Analysis of the position of the diffraction peaks indicates the formation of crystalline zeolite LTA, thus confirming the porous nature of the generated particles (inset of Figure 7B).

The obtained results confirm how nanocolloid precursors offer, from a molecular point of view, favorable conditions for the

self-assembly processes involved in the synthesis of hybrid matrixes.^{31–35} In this respect, soft interaction involved in the sol–gel process as well as the high adaptability to the reaction conditions reveals the very promising properties that amphiphilic templates can offer in the design and construction of hybrid inorganic–organic functional materials based on zeolites.^{10,36–39} Clearly, the presence of micellar block copolymers provides a steric stabilization that induces a transient colloidal stability to the synthesis environment.

Recently, transient colloidal stability has been suggested to be a controlling mechanism for particle formation in mesoporous silica SBA-15 in the presence of Pluronic block copolymer.³⁹ In this case block copolymer micellar aggregates provide steric stabilization within the water–silica matrix. It has been shown how the association of silica species to the corona of the Pluronic micelles drives the formation of silica–Pluronic–water “flocs” followed by an oriented aggregation of flocs toward secondary particles and a final fusion into larger aggregates.

Successful synthesis of aluminophosphate zeolites SAPO-34 has been recently performed by our research group using 1.86 nm sized (amine-terminated) poly(amidoamine) dendrimers as templates.⁴⁰ In that case the charged amine spatial distribution near the dendrimer surface creates a long-range electrostatic interaction that strongly influences the long-range assembly conditions for the zeolite growth. In the present study the advantageous use of PDMS–PEO block copolymer as a template for the construction of hybrid inorganic–organic porous nanomaterials relies on the formation of micellar aggregates possessing highly ramified PEO chains, which are responsible for the formation of a network of water molecules all around the macromolecular template. This water coordination around the precursor aggregates promotes a steric stabilization that induces an enhanced colloidal stability in solution and a favorable adaptability for the growth of the aluminosilicate LTA zeolitic phase onto the copolymer substrate.

In Figure 8 the multistep mechanism of formation of the PDMS–PEO block copolymer templated hybrid submicrometer particles is proposed. In this case the first stage of the self-assembly process involves the association of aluminosilicate species into the corona region of the PDMS–PEO micellar aggregates with the formation of primary units with a core–shell morphology (Figure 8B). During this period, restricted to an initial time of 1–3 h, the core–shell structure of the particles does not show significant changes, while a progressive aggregation process among these units leads to the formation of extended secondary units (Figure 8C). Further cross-linking, fusion, and rearrangement of the secondary particles leads to the formation of final submicrometer aggregates with fractal characteristics (Figure 8D), as confirmed by SEM observations.

4. CONCLUSION

The formation of porous LTA zeolite submicrometer particles from a clear sol containing block copolymers as templating agents has been investigated by means of SAXS, SEM, EDX, and XRD experiments. During the early stage of the growth process the formation of primary units of 4.8 nm with a core–shell morphology is driven by the incorporation of the zeolite aluminosilicate components onto the surface of the nano-template. The shape transition of the SAXS curves occurring at times greater than 180 min indicates an aggregation process among primary units that leads to the formation of large clusters with sizes ranging between 100 and 300 nm. Analysis of the log–log plot of the SAXS spectra during the late stages of synthesis

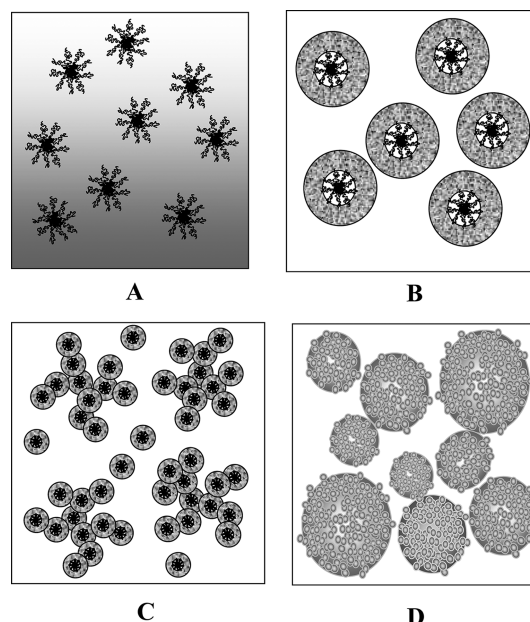


Figure 8. Sketch of the mechanism involved during the different stages of the synthesis of PDMS–PEO block copolymer templated hybrid submicrometer particles. The initial association of aluminosilicate species into the corona region of the PDMS–PEO micelles (A) generates primary units with a core–shell morphology (B), while a progressive aggregation process among these units leads to the formation of extended secondary structures (C). Further cross-linking, fusion, and rearrangement of the secondary particles leads to the formation of final submicrometer large aggregates (D).

indicates the presence of linear regions connected with fractal characteristics, both in mass and in the surface, of the generated aggregates. Generally, the driving interactions regulating the structure formation are difficult to understand, due also to the difficulty of following (*in situ*) the time evolution in a multicomponent complex environment. On the other hand, the use of a high molecular weight copolymer template seems to be an interesting possibility in place of more traditional templates. The use of block copolymers, in fact, allows the choice of the size and composition of the core substrate as well as modulation of the main features of the soft interaction at the boundary between organic and inorganic domains. Moreover, the presence of micellar block copolymers provides a steric stabilization that induces an enhanced (transient) colloidal stability to the synthesis environment. In this respect our results give important insights into the comprehension of the self-assembly processes involved in the development of organic–inorganic mesoporous matrixes, as well as stimulate the investigation of alternative protocols for the production of novel materials with new characteristics and properties.

■ AUTHOR INFORMATION

Corresponding Author

*Phone: +390903976222. Fax: +390903974130. E-mail: lombardo@me.cnr.it.

Notes

The authors declare no competing financial interest.

ACKNOWLEDGMENTS

We acknowledge the Società Sincrotrone Trieste for financial support for the experiment at the Elettra Synchrotron Radiation Facility.

REFERENCES

- (1) Tao, Y.; Kanoh, H.; Abrams, L.; Kaneko, K. Mesopore-Modified Zeolites: Preparation, Characterization, and Applications. *Chem. Rev.* **2006**, *106*, 896–910.
- (2) Jiang, J.-X.; Jordá, J. L.; Yu, J.; Baumes, L. A.; Mugnaioli, E.; Diaz-Cabañas, M. J.; Kolb, U.; Corma, A. Synthesis and Structure Determination of the Hierarchical Meso-Microporous Zeolite ITQ-43. *Science* **2011**, *333*, 1331–1334.
- (3) Fan, W.; Snyder, M. A.; Kumar, S.; Lee, P.-S.; Yoo, W. C.; McCormick, A. V.; Penn, R. L.; Stein, A.; Tsapatsis, M. Hierarchical Nanofabrication of Microporous Crystals with Ordered Mesoporosity. *Nat. Mater.* **2008**, *7*, 984–991.
- (4) Cho, K.; Na, K.; Kim, J.; Terasaki, O.; Ryoo, R. Zeolite Synthesis Using Hierarchical Structure-Directing Surfactants: Retaining Porous Structure of Initial Synthesis Gel and Precursors. *Chem. Mater.* **2012**, *24*, 2733–2738.
- (5) de la Escosura-Muñiz, A.; Merkoçi, A. Nanochannels Preparation and Application in Biosensing. *ACS Nano* **2012**, *6*, 7556–7583.
- (6) Jin, Y.; Li, Y.; Wang, H.; Zhao, S.; Lv, Z.; Du, X.; Sun, Y. Textural Mesoporosity and Opening Frame Network of Mesoporous MOR Zeolites Synthesized under Intensifying Perturbation Conditions. *Microporous Mesoporous Mater.* **2012**, *153*, 144–154.
- (7) Zhou, J.; Hua, Z.; Liu, Z.; Wu, W.; Zhu, Y.; Shi, J. Direct Synthetic Strategy of Mesoporous ZSM-5 Zeolites by Using Conventional Block Copolymer Templates and the Improved Catalytic Properties. *ACS Catal.* **2012**, *1*, 287–291.
- (8) Förster, S.; Antonietti, M. Amphiphilic Block Copolymers in Structure-Controlled Nanomaterial Hybrids. *Adv. Mater.* **1998**, *10*, 195–217.
- (9) Wu, Q. L.; Subramanian, N.; Rankin, S. E. Hierarchically Porous Titania Thin Film Prepared by Controlled Phase Separation and Surfactant Templating. *Langmuir* **2011**, *27*, 9557–9566.
- (10) Ghosh, S.; Saraswathi, A.; Indi, S. S.; Hoti, S. L.; Vasani, H. N. Ag–AgI, Core–Shell Structure in Agarose Matrix as Hybrid: Synthesis, Characterization, and Antimicrobial Activity. *Langmuir* **2012**, *28*, 8550–8561.
- (11) Cho, K.; Na, K.; Kim, J.; Terasaki, O.; Ryoo, R. Zeolite Synthesis Using Hierarchical Structure-Directing Surfactants: Retaining Porous Structure of Initial Synthesis Gel and Precursors. *Chem. Mater.* **2012**, *24*, 2733–2738.
- (12) Mallamace, F.; Beneduci, R.; Gambauro, P.; Lombardo, D.; Chen, S. H. Scaling Properties in the Internal Structure of Dendrimer Systems. *Physica A* **2002**, *304*, 235–243.
- (13) Merlitz, H.; He, G. L.; Wu, C. X.; Sommer, J.-U. Nanoscale Brushes: How To Build a Smart Surface Coating. *Phys. Rev. Lett.* **2009**, *102*, 115702 (1–4).
- (14) Chen, S. H.; Mallamace, F.; Faraone, A.; Gambauro, P.; Lombardo, D.; Chen, W. R. Observation of a Re-Entrant Kinetic Glass Transition in a Micellar System with Temperature-Dependent Attractive Interaction. *Eur. Phys. J. E* **2002**, *9*, 283–286.
- (15) Baulin, V. A.; Johner, A.; Avalos, J. B. Aggregation of Amphiphilic Polymers in the Presence of Adhesive Small Colloidal Particles. *J. Chem. Phys.* **2010**, *133*, 174905 (1–14).
- (16) Gao, F.; Hu, J.; Peng, C.; Liu, H.; Hu, Y. Synergic Effects of Imidazolium Ionic Liquids on P123 Mixed Micelles for Inducing Micro/Mesoporous Materials. *Langmuir* **2012**, *28*, 2950–2959.
- (17) Daful, A. G.; Baulin, V. A.; Avalos, J. B.; Mackie, A. D. Accurate Critical Micelle Concentrations from a Microscopic Surfactant Model. *J. Phys. Chem. B* **2011**, *115*, 3434–3443.
- (18) Zhlobenko, V. L.; Khodakov, A. Y.; Imperor-Clerc, M.; Durand, D.; Grillo, I. Initial Stages of SBA-15 Synthesis: An Overview. *Adv. Colloid Interface Sci.* **2008**, *142*, 67–74.
- (19) Manet, S.; Schmitt, J.; Imperor-Clerc, M.; Zhlobenko, V.; Durand, D.; Oliveira, C. L. P.; Pedersen, J. S.; Gervais, C.; Baccile, N.; Babonneau, F.; Grillo, I.; Meneau, F.; Rochas, C. Kinetics of the Formation of 2D-Hexagonal Silica Nanostructured Materials by Nonionic Block Copolymer Templating in Solution. *J. Phys. Chem. B* **2011**, *115*, 11330–11344.
- (20) Morelli, C.; Maris, P.; Sisci, D.; Perrotta, E.; Brunelli, E.; Perrotta, I.; Panno, M. L.; Tagarelli, A.; Versace, C.; Casula, M. F.; Testa, F.; Andò, S.; Nagy, J. B.; Pasqua, L. PEG-Templated Mesoporous Silica Nanoparticles Exclusively Target Cancer Cells. *Nanoscale* **2011**, *3*, 3198–3207.
- (21) Kim, Y.; Cho, C.-Y.; Kang, J.-H.; Cho, Y.-S.; Hyuk Moon, J. Synthesis of Porous Carbon Balls from Spherical Colloidal Crystal Templates. *Langmuir* **2012**, *28*, 10543–10550.
- (22) Zhulina, E. B.; Borisov, O. V. Theory of Block Polymer Micelles: Recent Advances and Current Challenges. *Macromolecules* **2012**, *45*, 4429–4440.
- (23) Barrer, R. M. *Zeolite and Clay Minerals as Sorbents and Molecular Sieves*; Academic Press: New York, 1978.
- (24) Barrer, R. M. *Hydrothermal Chemistry of Zeolites*; Academic Press: London, 1982.
- (25) Lombardo, D.; Micali, N.; Villari, V.; Kiselev, M. Large Structures in Diblock Copolymer Micellar Solution. *Phys. Rev. E* **2004**, *70*, 021402.
- (26) Amenitsch, H.; Bernstorff, S.; Kriechbaum, M.; Lombardo, D.; Mio, H.; Rappolt, M.; Laggner, P. Performance and First Results of the ELETTRA High-Flux Beamline for Small-Angle X-ray Scattering. *J. Appl. Crystallogr.* **1997**, *30*, 872–876.
- (27) Amenitsch, H.; Bernstorff, S.; Kriechbaum, M.; Lombardo, D.; Mio, H.; Pabst, G.; Rappolt, M.; Laggner, P. The Small-Angle X-ray Scattering Beamline at ELETTRA: A New Powerful Station for Fast Structural Investigations on Complex Fluids with Synchrotron Radiation. *Nuovo Cimento* **1999**, *20*, 2181–2190.
- (28) Chu, B. *Light Scattering. Basic Principle and Practice*; Academic Press: San Diego, CA, 1991.
- (29) Glatter, O.; Kratky, O. *Small-Angle X-ray Scattering*; Academic Press: London, 1982.
- (30) Schmidt, P. W. In *The Fractal Approach to Heterogeneous Chemistry: Surface, Colloids, Polymers*; Avnir, D., Ed.; Wiley: Chichester, U.K., 1989.
- (31) Pasqua, L.; Testa, F.; Aiello, R.; Cundari, S.; Nagy, J. B. Preparation of Bifunctional Hybrid Mesoporous Silica Potentially Useful for Drug Targeting. *Microporous Mesoporous Mater.* **2007**, *103*, 166–173.
- (32) Fan, W.; Snyder, M. A.; Kumar, S.; Lee, P.-S.; Yoo, W. C.; McCormick, A. V.; Penn, R. L.; Stein, A.; Tsapatsis, M. Hierarchical Nanofabrication of Microporous Crystals with Ordered Mesoporosity. *Nat. Mater.* **2008**, *7*, 984–991.
- (33) Bonaccorsi, L.; Lombardo, D.; Longo, A.; Proverbio, E.; Triolo, A. Dendrimer Template Directed Self-Assembly during Zeolite Formation. *Macromolecules* **2009**, *42*, 1239.
- (34) Fang, X.; Liu, Z.; Hsieh, M.-F.; Chen, M.; Liu, P.; Chen, C.; Zheng, N. Hollow Mesoporous Aluminosilica Spheres with Perpendicular Pore Channels as Catalytic Nanoreactors. *ACS Nano* **2012**, *6*, 4434–4444.
- (35) Liu, J.-Y.; Wang, J.-G.; Li, N.; Zhao, H.; Zhou, H.-J.; Sun, P.-C.; Chen, T.-H. Polyelectrolyte–Surfactant Complex as a Template for the Synthesis of Zeolites with Intracrystalline Mesopores. *Langmuir* **2012**, *28*, 8600–8607.
- (36) Liu, F.; Kong, W.; Qi, C.; Zhu, L.; Xiao, F.-S. Design and Synthesis of Mesoporous Polymer-Based Solid Acid Catalysts with Excellent Hydrophobicity and Extraordinary Catalytic Activity. *ACS Catal.* **2012**, *2*, 565–57.
- (37) Athens, G. L.; Kim, D.; Epping, J. D.; Cadars, S.; Ein-Eli, Y.; Chmelka, B. F. Molecular Optimization of Multiply-Functionalized Mesoporous Films with Ion Conduction Properties. *J. Am. Chem. Soc.* **2011**, *133*, 16023–16036.
- (38) Dai, H.; Yang, J.; Ma, J.; Chen, F.; Fei, Z.; Zhong, M. A Green Process for the Synthesis of Controllable Mesoporous Silica Materials. *Microporous Mesoporous Mater.* **2012**, *147*, 281–285.

(39) Ruan, J.; Kjellman, T.; Sakamoto, Y.; Alfredsson, V. Transient Colloidal Stability Controls the Particle Formation of SBA-15. *Langmuir* **2012**, *28*, 11567–11574.

(40) Bonaccorsi, L.; Calandra, P.; Amenitsch, H.; Proverbio, E.; Lombardo, D. Growth of Fractal Aggregates during Template Directed SAPO-34 Zeolite Formation. *Microporous Mesoporous Mater.* **2013**, *167*, 3–9.